ELSEVIER

Biophysical Chemistry 52 (1994) 1–13

Biophysical Chemistry

# Analysis of anisotropy decays in terms of correlation time distributions, measured by frequency-domain fluorometry

Ignacy Gryczynski [a], Michael L. Johnson [b], Joseph R. Lakowicz [a]

[a] *University of Maryland School of Medicine, Center for Fluorescence Spectroscopy, Department of Biological Chemistry, 108 N. Greene Street, Baltimore, MD 21201, USA*

[b] *University of Virginia, Department of Pharmacology, Box 448, Charlottesville, VA 22908, USA*

Received 30 August 1993; accepted in revised form 21 January 1994

**Abstract**

We describe the theory and practical aspects of analyzing fluorescence anisotropy decays in terms of correlation times distributions. In our model the rotational motions of the fluorophores were described using Gaussian or Lorentzian distributions of the correlation times. The theory is presented both for time and frequency-domain measurements, although the simulations and measurements are focused on the frequency-domain measurements of the anisotropy decays. Analysis of simulated data is presented to illustrate the nature of the data and the resolution which can be expected with presently available frequency-domain measurements. Additionally, we describe experimental data for samples where one can reasonably expect a single exponential and/or discrete multi-exponential correlation time distributions, and for samples where the anisotropy decay might be expected to display a distribution of correlation times. These samples include small single tryptophan peptides in propylene glycol, the single tryptophan residue in S. Nuclease, and the single tryptophan residue in the native and partially unfolded states of ribonuclease $T_1$.

*Key words:* Fluorescence; Anisotropy; Frequency domain; Fluorometry; Correlation time distribution

## 1. Introduction

Time-dependent decays of fluorescence anisotropy can reveal the size, shape and flexibility of biological macromolecules [1–6]. Such decays are generally analyzed in terms of the multi-correlation time or multi-exponential model, in which the time-dependent anisotropy is assumed to decay as a sum of exponentials. This is a reasonable model for many systems. For instance, spheres, ellipsoids of revolution, asymmetric ellipsoids and rigid asymmetric molecules are all expected to display a multi-exponential anisotropy decay with one to five discrete correlation times [1–4]. However, anisotropy decays can be expected to be more complex for molecules which display flexing or segmental motions in addition to rotational diffusion, or structures in which the fluorophore

Abbreviations: CTD, correlation time distribution; FD, frequency-domain; FDA, frequency-domain anisotropy; Gau, Gaussian distribution; hw, full-width at half maximum, half-width; Lor, Lorentzian distribution; NATE, N-acetyl-L-tryptophan, ethyl ester; Pentagastrin, N-t-BOC-b-ala-trp-met-asp-phe-amide; RNase $T_1$, ribonuclease $T_1$; TD, time-domain.


*SSDI* 0301-4622(94)00031-E

is present in a restricted and/or asymmetric environment. For instance, the anisotropy decay of fluorophores intercalated into double-helical DNA are expected to be more complex than a multi-exponential i.e. non-exponential, due to the torsional and bending motions of the DNA which occur on a number of timescales [7–15]. Similarly, the anisotropy decays of membrane-bound fluorophores, which may experience a hindered or anisotropic environment, are also expected to be non-exponential [16–19].

The tryptophyl residues of proteins are present in a variety of environments, ranging from fully shielded by a rigid protein matrix to fully exposed to the aqueous phase [20]. Because these residues exist in a hindered dynamic environment, it seems likely that these residues will display a variety of motions, with various amplitudes and correlation times. Consequently, it may be informative to interpret the anisotropy decays of proteins in terms of correlation time distributions. To date, protein anisotropy decays have been successfully analyzed in terms of the multi-exponential model [20–28], which is to be expected given the power of the multi-exponential model for approximating complex decay processes. However, it is likely that proteins display a variety of motions, ranging from rapid low amplitude motions of individual amino acids or portions thereof, to somewhat slower motions of groups of amino acids and/or protein domains. Indeed, molecular dynamics simulations have suggested the existence of a range of characteristic times and amplitudes for protein motions [29,30], and others have suggested that the dynamics may be fractal [31,32]. Hence, the use of correlation time distributions (CTD) may provide valuable insights into the complex dynamic properties of proteins, membranes and nucleic acids, and may allow visualization of changes in protein dynamics in response to solution conditions which effect protein stability.

The use of correlation time distribution is an extension of similar studies in which fluorescence intensity decays have been analyzed in terms of decay time distributions [33–39]. We used analytical forms for the distribution functions to minimize the number of variable parameters. In particular we used Gaussian (Gau) and Lorentzian (Lor) correlation time distributions. The present paper emphasizes frequency-domain measurements, which are now known to provide impressive resolution of complex anisotropy decays [40]. The resolution of the frequency-domain (FD) measurements can be increased further by measurements in the presence of varying amounts of collisional [41] or energy transfer quenchers [42], followed by global analysis of the multiple data sets [43,44]. Our data suggest that the anisotropy decays of flexible peptides in various solvents are in fact well described by distributions of correlation times. The anisotropy decay of RNase $T_1$ in the native state appears to be a single correlation time, which becomes a distribution of correlation times as the protein is unfolded by heat or denaturation.

## 2. Theory

Fluorescence anisotropy decays are most often described as a sum of individual exponentials. Following $\delta$-function excitation the time-dependent anisotropy is given by

$$r(t) = \sum_j r_{0j} \exp(-6R_j t) = \sum_j r_{0j} \exp(-t/\theta_j), \quad (1)$$

where $r_{0j}$ are the amplitudes, $R_j$ the rotational rates, and $\theta_j = (6R_j)^{-1}$ the correlation time of the $j$th component. The fraction of the total anisotropy which decays by each correlation time is

$$g_j = \frac{r_{0j}}{\sum_k r_{0k}} = \frac{r_{0j}}{r_0}. \quad (2)$$

The object of the multi-exponential analysis is to fit the data in terms of the amplitudes ($r_{0j}$) and the correlation times ($\theta_j$). Two variations are possible. The total anisotropy can be considered to be unknown, in which case there are $j$ variable amplitudes. Alternatively, the total anisotropy in the absence of rotational motions ($r_0$) can be determined from a separate experiment, such as

measurements at low temperature and/or high viscosity where rotational diffusion does not occur during the lifetime of the excited state. In this case there are $j-1$ unknown amplitudes with $\Sigma_j g_j = 1.0$ or $\Sigma_j r_{0j} = r_0$.

We now consider a distribution of correlation times, but it should be noted that similar expressions are easily written for distributions of rotational rates. In the present paper we are not considering the molecular interactions which result in the distributions, and such future consideration may clarify the selection of rotational rate or correlation time distribution. Because of the limited resolution of the experimental data it is necessary to use distribution functions with a reasonably small number of variable parameters. Hence, we arbitrarily selected Gaussian (G), Lorentzian (L) and rectangular (R) distributions. For these functions the correlation times are distributed according to

$$p^{\mathrm{G}}(\theta) = \frac{1}{\sigma\sqrt{2\pi}} \exp\left[ -\frac{1}{2}\left( \frac{\theta - \bar{\theta}}{\sigma} \right)^2 \right], \tag{3}$$

$$P^{\mathrm{L}}(\theta) = \frac{1}{\pi} \frac{\Gamma/2}{(\theta - \bar{\theta})^2 + (\Gamma/2)^2}, \tag{4}$$

$$P^{\mathrm{R}}(\theta) = 1/\Gamma \text{ for } \theta_{\mathrm{L}} \leqslant \theta \leqslant \theta_{\mathrm{U}},$$

$$= 0 \text{ for } \theta < \theta_{\mathrm{L}} \text{ and } \theta > \theta_{\mathrm{U}}. \tag{5}$$

In these expressions $\bar{\theta}$ are the central values, $\sigma$ the standard deviation of the Gaussian, $\Gamma$ the full-width at half-maximum amplitude of the Lorentzian, and $\theta_{\mathrm{L}}$ and $\theta_{\mathrm{U}}$ are the lower and upper limits of the rectangular distribution. For consistency we will present all widths as the half-width (hw, $\Gamma$), which is the full-width at half-maximum amplitude. For a Gaussian $\Gamma = 2.354\ \sigma$ [45]. During analysis these functions are all normalized to unity if integrated from zero to plus infinity. In the figures these shape factors are shown as peak-normalized.

Suppose the anisotropy decay is described by a single modal correlation time distribution (CTD) with a single mean value ($\bar{\theta}$), width (hw) and amplitude ($r_0$). That part of the anisotropy decay which displays a correlation time $\theta$ is given by

$$r(t, \theta) = r_0 P(\theta)\ \mathrm{e}^{-t/\theta}. \tag{6}$$

However, one cannot selectively observe this component of the anisotropy decay, but rather must observe all the components. Hence, the observed anisotropy is given by the integral equation

$$r(t) = r_0 \int_{\theta=0}^{\infty} P(\theta)\ \mathrm{e}^{-t/\theta}\ \mathrm{d}\theta. \tag{7}$$

By analogy with Eq. (1) it is possible that the CTD could be multimodal, that is, be described by more than a single Gaussian, Lorentzian or rectangle. Then, the amplitude of the anisotropy decay which has a correlation time $\theta$ is given by

$$r(t, \theta) = \sum_j r_{0j} P_j(\theta)\ \mathrm{e}^{-t/\theta}, \tag{8}$$

where the sum accounts for the contribution at $\theta$ from each mode of the distribution, and $r_{0j}$ is the amplitude associated with the $j$th mode of the distribution. In this case each normalized distribution is characterized by the appropriate parameters, $\bar{\theta}_j$, $\mathrm{hw}_i$, $\Gamma_i$. The observed anisotropy is given by

$$r(t) = \sum_j r_{0j} \int_{\theta=0}^{\infty} P_j(\theta)\ \mathrm{e}^{-t/\theta}\ \mathrm{d}\theta. \tag{9}$$

We note that the distribution shape factors $P_j(\theta)$ are normalized such that the integrated probability of each mode of the distribution is equal to unity. This becomes important when part of the distribution occurs at $\theta < 0$. Hence, the $P_j(\theta)$ in Eqs. (6)–(9) are normalized using

$$P_j(\theta) = \frac{P'_j(\theta)}{\int_{\theta=0}^{\infty} P'_j(\theta)\ \mathrm{d}\theta}, \tag{10}$$

where the $P'_j(\theta)$ values are those prior to normalization. With this normalization the $r_{0j}$ values in Eqs. (8) or (9) indicate the amplitude of the anisotropy which is associated with the $j$th mode of the distribution centered at $\bar{\theta}_j$.

### 2.1. Frequency-domain anisotropy decays

The FD anisotropy decay analysis is most clearly presented in terms of the total intensity

decay ($I(t)$) and the intensity decays of the parallel ($\|$) and perpendicularly polarized ($\perp$) components of the emission. These intensity decays are related by

$$I(t) = I_{\|}(t) + 2I_{\perp}(t) = \sum_i \alpha_i \, e^{-t/\tau_i} = \sum_i \alpha_i \, e^{-\Gamma_i t}, \quad (11)$$

$$I_{\|}(t) = \tfrac{1}{3} I(t)[1 + 2r(t)], \quad (12)$$

$$I_{\perp}(t) = \tfrac{1}{3} I_{\|}(t)[1 - r(t)]. \quad (13)$$

The total intensity decay can be analyzed in terms of a multi-exponential decay (Eq. (11)) where $\alpha_i$ are the pre-exponential factors, $\tau_i$ the decay times and $\Gamma_i$ the decay rates. We generally measure $I(t)$ in a separate experiment using magic angle polarization conditions. It is also possible to analyze the intensity decay in terms of decay-time distributions, but this is not necessary for the CTD analysis. Analysis of the FD anisotropy data requires an accurate description of the time-dependent decay [27], which is readily accomplished during the multi-exponential model (Eq. (11)). This use of a multi-exponential intensity decay does not introduce any new parameters into the anisotropy decay analysis because the values of $\alpha_i$ and $\tau_i$ are held fixed in the anisotropy analysis.

The parameters describing the anisotropy decay are determined by non-linear least-squares [45], as has been described previously for multiexponential intensity [46] and anisotropy decays [47,48]. In the frequency-domain the measured quantities for the anisotropy analysis are the phase angle difference between the perpendicular and parallel components of the polarized emission ($\Delta_\omega$) and the ratio of the amplitude of the polarized and modulated emission ($\Lambda_\omega$) each measured over a range of modulation frequencies ($\omega$). The values of $\Delta_\omega$, and $\Lambda_\omega$ can be calculated [48,49] using

$$\Delta_{c\omega} = \arctan\left(\frac{D_{\|}N_{\perp} - N_{\|}D_{\perp}}{N_{\|}N_{\perp} + D_{\|}D_{\perp}}\right), \quad (14)$$

$$\Lambda_{c\omega} = \left(\frac{N_{\|}^2 + D_{\|}^2}{N_{\perp}^2 + D_{\perp}^2}\right)^{1/2} \quad (15)$$

where

$$N_P = \int_{t=0}^{\infty} I_P(t) \sin \omega t \, dt \quad (16)$$

$$D_P = \int_{t=0}^{\infty} I_P(t) \cos \omega t \, dt, \quad (17)$$

and P indicates the polarization ($\|$ or $\perp$). The parameters describing the experimental anisotropy decay are obtained by minimization of

$$\chi_R^2 = \frac{1}{\nu}\sum_{\omega}\left(\frac{\Delta_\omega - \Delta_{c\omega}}{\delta\Delta}\right)^2 + \frac{1}{\nu}\sum_{\omega}\left(\frac{\Lambda_\omega - \Lambda_{c\omega}}{\delta\Lambda}\right)^2, \quad (18)$$

where $\delta\Delta$ and $\delta\Lambda$ are the experimental uncertainties in $\Delta_\omega$ and $\Lambda_\omega$. For simulated data we use Gaussian distributed noise with $\delta\Delta = 0.2°$ and $\delta\Lambda = 0.005$.

The transforms could be written in double integral form using Eqs. (9), (13), (16) and (17). However, for purposes of calculation we prefer a more explicit representation [48]. For a multi-exponential intensity and anisotropy decay the transforms are given by

$$N_{\|} = \tfrac{1}{3}A + \tfrac{2}{3}B, \quad (19)$$

$$N_{\perp} = \tfrac{1}{3}A - \tfrac{1}{3}B, \quad (20)$$

$$D_{\|} = \tfrac{1}{3}C + \tfrac{2}{3}D, \quad (21)$$

$$D_{\perp} = \tfrac{1}{3}C - \tfrac{1}{3}D, \quad (22)$$

with

$$A = \sum_i \frac{\alpha_i \omega}{\omega^2 + \Gamma_i^2}, \quad (23)$$

$$B = \sum_i \alpha_i \omega \sum_j \frac{r_{0j}}{\omega^2 + (\Gamma_i + 6R_j)^2} \quad (24)$$

$$C = \sum_i \frac{\alpha_i \Gamma_i}{\omega^2 + \Gamma_i^2}, \quad (25)$$

$$D = \sum_i \alpha_i \sum_j \frac{r_{0j}(\Gamma_i + 6R_j)}{\omega^2 + (\Gamma_i + 6R_j)^2}. \quad (26)$$

For a distribution of correlation times terms $A$ and $C$ are unchanged, and by analogy

$$B = \sum_i \alpha_i \omega \int_{\theta=0}^{\infty} \sum_j \frac{r_{0j} P_j(\theta)\, \mathrm{d}\theta}{\omega^2 + (\Gamma_i + 6R_j)^2} \tag{27}$$

$$D = \sum_i \alpha_i \int_{\theta=0}^{\infty} \sum_j \frac{r_{0j} P_j(\theta)(\Gamma_i + 6R_j)\, \mathrm{d}\theta}{\omega^2 + (\Gamma_i + 6R_j)^2}, \tag{28}$$

where $P_j(\theta)$ are the normalized distributions. The FD polarized modulation data are presented as modulated anisotropies

$$m_\omega = \frac{\Lambda_\omega - 1}{\Lambda_\omega + 2}. \tag{29}$$

### 2.2. Lifetime distribution analysis of the intensity decays

During our analysis of the intensity decays of peptides in propylene glycol we noticed that these data could be well fit using distributions of decay times. This analysis was performed as described previously [39]. Briefly, the pre-exponential factors are assumed to be Gaussian or Lorentzian.

$$\alpha_G(\tau) = \frac{1}{\sigma\sqrt{2\pi}} \exp\left[ -\frac{1}{2}\left( \frac{\tau - \bar{\tau}}{\sigma} \right)^2 \right], \tag{30}$$

$$\alpha(\tau) = \frac{1}{\pi} \frac{\Gamma/2}{(\tau - \bar{\tau})^2 + (\Gamma/2)^2}, \tag{31}$$

where $\bar{\tau}$ is the central value of the distribution, $\sigma$ the standard deviation of the Gaussian, and $\Gamma$ the full-width at half-maximum (fw) for the Lorentzian, not to be confused with the decay rates $\Gamma_i$.

The parameters describing the decay time distribution, or the $\alpha_i$ and $\tau_i$ values in Eq. (11), are determined by nonlinear least-squares. For the decay time distribution the calculated phase angles ($\phi_\omega$) and modulation values ($m_\omega$) are given by

$$\phi_c = \arctan\left( \frac{N_\omega}{D_\omega} \right), \tag{32}$$

$$m_{c\omega} = \left( N_\omega^2 + D_\omega^2 \right)^{1/2}, \tag{33}$$

where

$$N_\omega J = \int_{\tau=0}^{\infty} \frac{\alpha(\tau)\omega\tau^2}{1 + \omega^2\tau^2} \mathrm{d}\tau, \tag{34}$$

$$D_\omega J = \int_{\tau=0}^{\infty} \frac{\alpha(\tau)\tau}{1 + \omega^2\tau^2} \mathrm{d}\tau, \tag{35}$$

with

$$J = \int_{\tau=0}^{\infty} \alpha(\tau)\tau \, \mathrm{d}\tau. \tag{36}$$

## 3. Materials and methods

Frequency-domain measurements were performed on the GHz harmonic content instrument described previously [50,51]. The excitation source was a cavity-dumped R6G dye laser (Coherent 702-2), whose output was frequency doubled to 295–300 nm. The pulse widths were about 8 ps, with a cavity-dumped rate of 3.79 MHz. The dye laser was pumped with about 800 mW of 514 nm light, from a mode-locked argon ion laser (Coherent Innova 15). The detector was a microchannel plate PMT, Hamamatsu R1564U. The tryptophan emission was isolated using a WG320 filter, which transmits wavelengths above 320 nm. The samples were excited at 300 nm.

NATE was from Bachem Inc., the di and tripeptides, gastrin and pentagastrin were from Sigma, and all were used without further purification. RNase $T_1$ was a gift from M. Eftink, University of Mississippi, and S. Nuclease was a gift from L. Brand, The Johns Hopkins University. Acrylamide was from BioRad, electrophoresis grade, greater than 99.9% pure.

## 4. Results and discussion

### 4.1. Simulations

We questioned the form of the FD anisotropy data for a distribution of correlation times, as compared with that resulting from a multi-exponential decay. Simulated FD anisotropy data

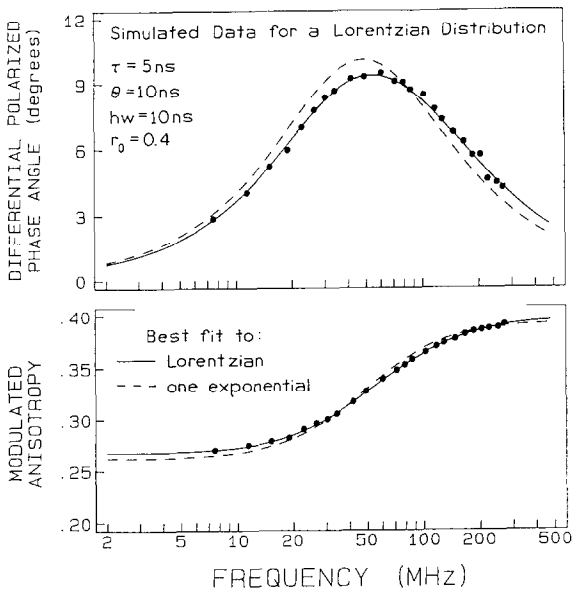


Fig. 1. Simulated frequency-domain anisotropy data for a Lorentzian distribution of correlation times. For comparison we show a best single correlation time (– – –). The parameter values used for the simulation were $\tau = 5$ ns, $\bar{\theta} = 10$ ns, hw = 10 ns, $r_0 = 0.40$. The simulated data contain Gaussian noise $\delta\Delta = 0.2°$ and $\delta\Lambda = 0.005$.

for a Lorentzian correlation time distribution are shown in Fig. 1. For these simulations we assumed a decay time of 5 ns, a most probable correlation time of $\bar{\theta} = 10$ ns, and half width of 10 ns. The differential phase profile is mostly symmetric and visually similar to the shape known for single correlation time. Analysis of these simulated data in terms of the Lorentzian distribution model results in recovery of the expected parameter values. However, the best single correlation time fit (dashed curve) yielded an unacceptable value of $\chi^2_R = 15$ (Table 1 and Fig. 1). However, it does not seem possible to distinguish the shapes of the distributions, since analysis with the Gaussian model yielded an acceptable value with $\chi^2_R = 1.07$. The two correlation time model also yielded an acceptable fit, and it would be difficult in practice to reject this model. As seen from Table 1, the Gaussian correlation time distribution and two correlation time models both provide good fits to the simulated Lorentzian distribution. While it is thus possible to distinguish a wide distribution of correlation times from a single correlation time, it does not appear practical to resolve such a distribution from a multi-exponential anisotropy decay. It is interesting to note that the two correlation time analysis yielded a second correlation time near 2 ns. This probably results from the assumed fluorescence lifetime of 5 ns, which results in most of the information content being available for correlation times near this value.

We also simulated data for a double exponential anisotropy decay (Fig. 2), and questioned whether such decays could be mistaken for a distribution of correlation times. In this simulation we assumed that each correlation time contributed an equal amplitude to the anisotropy decay ($r_{01} = r_{02} = 0.2$). If the correlation times are very different (1 and 15 ns), then each correlation time makes visible contributions to the FD data (Fig. 2). This is seen from the less symmetric profile of the differential phase angles (compared with Fig. 1). We were surprised to find that the simulated multi-exponential anisotropy data cannot be fit to a unimodal distribution of correlation times, either to Lorentzian (Fig. 2, dashed curve) or Gaussian (Fig. 2, dotted curve). The double exponential anisotropy decay with widely spaced correlation times (1 and 15 ns) cannot be fitted by Lorentzian ($\chi^2_R = 31.1$) or Gaussian model ($\chi^2_R = 98.0$). However, if the correlation times are more closely spaced, 5 and 10 ns, then it is difficult to distinguish two distinct correlation

Table 1
Analysis of simulated data for a Lorentzian distribution of correlation times [a]

| Model [b] | $\bar{\theta}$ (ns) | hw (ns) | $r_i$ | $\chi^2_R$ |
|---|---|---|---|---|
| Lorentzian [a] | 9.89 | 10.33 | 0.40 | 0.94 |
| Gaussian | 11.86 | 18.06 | 0.40 | 1.07 |
| 1 exponential | 10.14 | – | 0.39 | 15.24 |
| 2 exponential | 2.34 | – | 0.06 | – |
| | 13.45 | – | 0.34 | 1.19 |

[a] The data were simulated for $\bar{\theta} = 10$ ns, hw = 10 ns, $r_0 = 0.40$, and $\tau = 5$ ns, for a Lorentzian distribution of decay times. Random noise was added to the simulated values, $\delta\Delta = 0.2°$ and $\delta\Lambda = 0.005$.

[b] Model used to analyze the simulated data.

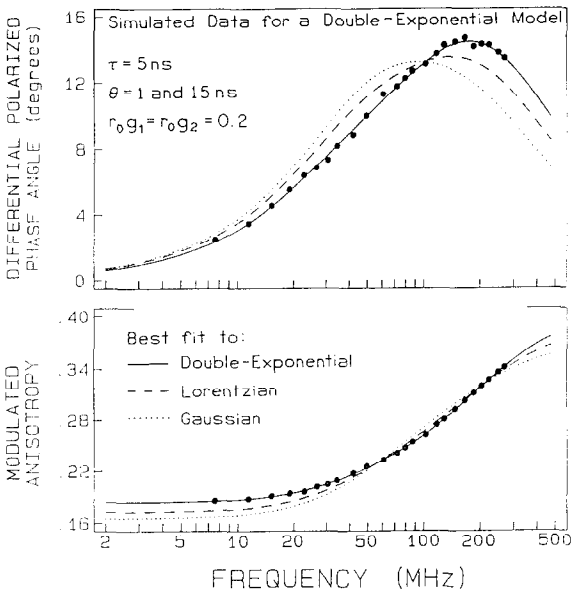


Fig. 2. Simulated frequency-domain data (•) for a two correlation time anisotropy decay. The parameter values are $\tau = 5$ ns, $\theta_1 = 1$ ns, $\theta_2 = 15$ ns, $r_{01} = r_{02} = 0.2$. Also shown are the best fits to a single modal Lorentzian (– – –) and single-modal Gaussian (· · · · · ·) distribution of correlation times.

Table 2
Analysis of simulated data for a double exponential anisotropy decay [a]

| Model [b] | $\bar{\theta}$ (ns) | hw (ns) | $r_0$ | $\chi^2_R$ |
|---|---|---|---|---|
| 2 exponential | 1.01 | – | 0.20 | – |
| (1 and 15 ns) [c] | 15.2 | – | 0.20 | 0.095 |
| Lorentzian | −2.83 | 2.82 | 0.42 | 31.1 |
| Gaussian | −26.1 | 32.5 | 0.39 | 98.0 |
| 2 exponential [a] | 5.6 | – | 0.27 | |
| (5 and 10 ns) [c] | 13.1 | – | 0.13 | 1.00 |
| Lorentzian | 7.0 | 1.33 | 0.40 | 1.07 |
| Gaussian | 7.3 | 4.90 | 0.40 | 1.03 |

[a] The simulated data are for two correlation times, $\theta_1 = 1$ ns, and $\theta_2 = 15$ ns; or $\theta_1 = 5$ ns and $\theta_2 = 10$ ns. In both cases, $r_{01} = r_{02} = 0.20$, $\tau = 5$ ns.
[b] Model used to analyze the simulated data.
[c] Values in parentheses are the correlation times used for the simulation.

times from a single distribution of correlation times (Table 2).

### 4.2. Single tryptophan peptides

We examined a number of single-tryptophan peptides in propylene glycol. These peptides range from the neutral tryptophan derivative NATE, to tripeptides with a central tryptophan residue and various sized adjacent amino acids, to the tetra- and penta-peptides gastrin and pentagastrin, respectively. We reasoned that these peptides would display a range of correlation times due to their intrinsic conformation flexibility and differing global rotational rates for the different conformations. Propylene glycol was selected as the solvent to provide overall correlation times of 5–10 ns, which are easily measured with our instrumentation, which are reasonably near the tryptophan intensity decay times, and which are typical of the overall correlation times of globular proteins.

Frequency-domain anisotropy data for one representative peptide, leu-trp-leu, are shown in Fig. 3. These data are well fit with a broadly distributed Lorentzian (Fig. 4). However, it is also possible to fit the data using the two correlation time model (Tables 3 and 4). Similar results were

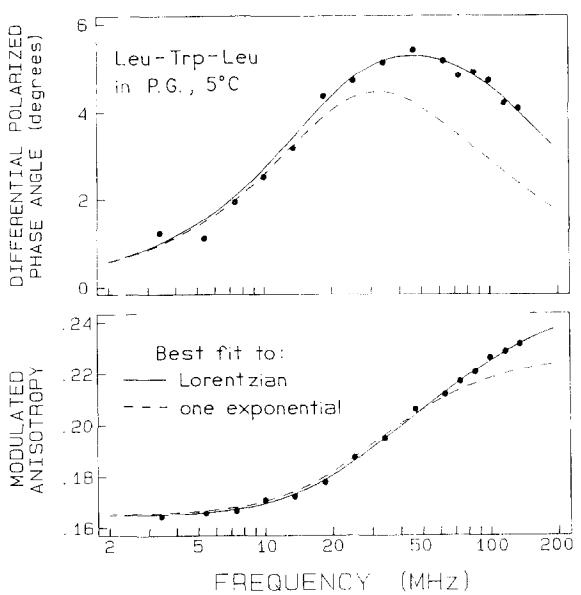


Fig. 3. Frequency-domain anisotropy data for Leu-Trp-Leu. The solid line shows the best fit to a Lorentzian correlation time distribution, and the dashed line the best fit to a single correlation time.

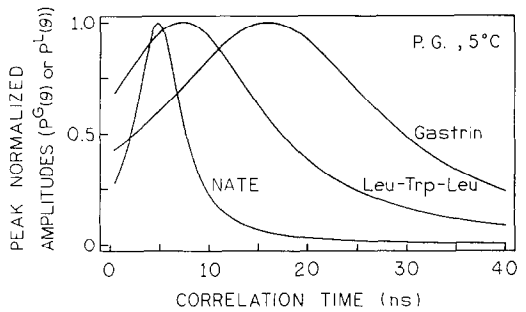


Fig. 4. Correlation time distributions for single tryptophan peptides.

obtained for peptides ranging from a single amino acid NATE, several tripeptides, gastrin (four amino acids) and pentagastrin (five amino acids). In the case of NATE it is probable that the width of the distribution is due to a combination of limited resolution, as well as non-isotropic rotational diffusion. In each case the FD data are equally well fit using a unimodal correlation time distribution and the two correlation time model. Representative correlation time distributions are plotted in Fig. 4. Given the structural heterogeneity of the peptides it seems probable that the underlying anisotropy decays are in fact the result of distribution of the types shown in Fig. 4. The average correlation times $\bar{\theta}$ evidently depends on molecular weight of peptide, the shortest being gly-Trp (MW = 279) and the longest being gastrin and pentagastrin (MW = 633 and 858, respectively).

Table 3
Multi-exponential analysis of anisotropy decays of small peptides in propylene glycol at 5°C

| Model | $\theta_i$ [a] (ns) | $r_0 g_i$ [a] | $1\theta$ [b] | $2\theta$ |
|---|---|---|---|---|
| NATE | 2.72 | 0.109 | | |
| | 10.73 | 0.140 | 11.4 | 1.1 |
| Gly-Trp | 2.39 | 0.091 | | |
| | 11.73 | 0.153 | 17.6 | 2.5 |
| Gly-Trp-Gly | 3.31 | 0.080 | | |
| | 21.70 | 0.168 | 17.6 | 0.5 |
| Leu-Trp-Leu | 2.96 | 0.064 | | |
| | 20.40 | 0.182 | 20.7 | 2.0 |
| Glu-Trp-Glu | 3.12 | 0.061 | | |
| | 18.86 | 0.186 | 13.3 | 1.4 |
| Lys-Trp-Lys | 3.12 | 0.033 | | |
| | 20.73 | 0.217 | 6.6 | 0.8 |
| Gastrin | 4.63 | 0.054 | | |
| | 29.98 | 0.195 | 4.9 | 0.8 |
| Pentagastrin | 3.39 | 0.038 | | |
| | 29.65 | 0.211 | 9.4 | 1.6 |

[a] The parameters listed are for the two correlation time ($2\theta$) fit.
[b] This is the $\chi^2_R$ value for the one correlation time ($1\theta$) fit. The parameters from this fit are not shown.

Table 4
Distribution analysis (Lorentzian unimodal) of anisotropy decays of small peptides in propylene glycol at 5°C

| Compound | $\bar{\theta}$ (ns) | $\Gamma$ (ns) | $r_0$ | $\chi^2_R$ |
|---|---|---|---|---|
| NATE | 4.91 | 5.72 | 0.254 | 1.1 |
| Gly-Trp | 4.72 | 8.52 | 0.250 | 2.3 |
| Gly-Trp-Gly | 6.74 | 19.74 | 0.253 | 0.5 |
| Leu-Trp-Leu | 7.14 | 21.59 | 0.251 | 1.7 |
| Glu-Trp-Glu | 8.94 | 17.60 | 0.251 | 1.3 |
| Lys-Trp-Lys | 12.85 | 18.00 | 0.252 | 0.8 |
| Gastrin | 16.00 | 27.14 | 0.252 | 0.8 |
| Pentagastrin | 14.47 | 38.87 | 0.252 | 1.6 |

The anisotropy decay analysis requires knowledge of the intensity decays, which for completeness are summarized in Table 5. We note that these intensity decays are also equally well fit to a lifetime distribution (Table 6) as to a sum of exponentials (Table 5).

### *4.3. Global analysis of the S. Nuclease anisotropy decay*

We previously demonstrated that collisional quenching can be used to increase the resolution of the FDA measurements [40,41]. More specifically, quenching alters the mean decay time, and hence the contributions of each correlation time to the anisotropy data. Global analysis of the FDA data, measured over a range of decay times, provides enhanced resolution of the anisotropy decay. We applied this method to S. Nuclease, which contain a single tryptophan residue. By acrylamide quenching we were able to reduce the mean decay time from 5.8 to 1.3 ns (Table 7).

Global anisotropy decay analyses are presented in Table 8. The anisotropy decay of the single tryptophan residue in S. Nuclease (Fig. 5) is nearly a single exponential, yielding $\chi^2_R = 2.0$.

Table 5
Multi-exponential analysis of intensity decay of small peptides in propylene glycol at 5°C

| Compound | $\tau_i$ (ns) | $\alpha_i$ [a] | $f_i$ [b] | $\chi^2_R$ | |
|---|---|---|---|---|---|
| | | | | 1 exp | 2 exp |
| NATE | 2.15 | 0.531 | 0.282 | | |
| | 6.19 | 0.469 | 0.718 | 132.8 | 1.2 |
| Gly-Trp | 2.59 | 0.498 | 0.275 | | |
| | 6.76 | 0.502 | 0.725 | 90.3 | 0.8 |
| Gly-Trp-Gly | 2.16 | 0.560 | 0.290 | | |
| | 6.73 | 0.440 | 0.710 | 185.6 | 1.1 |
| Leu-Trp-Leu | 2.61 | 0.434 | 0.229 | | |
| | 6.78 | 0.566 | 0.771 | 74.4 | 1.3 |
| Glu-Trp-Glu | 2.39 | 0.444 | 0.236 | | |
| | 6.18 | 0.556 | 0.769 | 77.4 | 1.5 |
| Lys-Trp-Lys | 2.49 | 0.416 | 0.213 | | |
| | 6.58 | 0.584 | 0.787 | 76.9 | 1.0 |
| Gastrin | 2.18 | 0.554 | 0.317 | | |
| | 5.83 | 0.446 | 0.683 | 111.3 | 1.6 |
| Pentagastrin | 2.47 | 0.456 | 0.229 | | |
| | 6.96 | 0.544 | 0.771 | 16.6 | 1.4 |

[a] The $\alpha_i$ values are the pre-exponential factors in the multi-exponential fit of the intensity decay data, $I(t) = \sum\alpha_i \exp(-t/\tau_i)$.
[b] The fractional contribution of each component to the total emission is given by $f_i = \tau_i / \sum\alpha_j\tau_i$.

The double correlation time model results in a modest decrease in $\chi^2_R$ to 1.0, which is significant given the number of data points or degrees of freedom (about 300). The shorter correlation time near 0.09 ns displays only a small amplitude. Both the Lorentzian and Gaussian correlation time distribution models also provide reasonable fits to the data. The well defined position of the tryptophan within the rigid protein results in relatively sharp correlation time distribution (hw = 2.7 ns, Fig. 6). In spite of this modest width, non-zero widths are required by the data, as seen by the increased values of $\chi^2_R$ when the widths are held constant near zero (Table 8). It seems likely that such widths will be sensitive to the structural and dynamic feature which surround tryptophan residues in proteins.

It is interesting and informative to compare the correlation time distributions of S. Nuclease recovered using the Lorentzian or Gaussian models. The distribution from the Gaussian model is considerably wider than that from the Lorentzian model (Fig. 6). In our opinion, this is a result of the wings of a Lorentzian, which extend well

Table 6
Lorentzian lifetime distribution analysis of the intensity decays of small peptides, propylene glycol, 5°C

| Compound | $\bar{\tau}$ (ns) | hw (ns) | $\chi^2_R$ |
|---|---|---|---|
| NATE | 3.25 | 3.67 | 1.1 |
| Gly-Trp | 4.08 | 3.95 | 0.8 |
| Gly-Trp-Gly | 2.97 | 4.92 | 0.7 |
| Leu-Trp-Leu | 4.50 | 3.86 | 1.2 |
| Glu-Trp-Glu | 4.03 | 3.12 | 1.1 |
| Lys-Trp-Lys | 4.42 | 3.67 | 1.2 |
| Gastrin | 3.20 | 2.79 | 1.4 |
| Pentagastrin | 4.25 | 4.85 | 1.0 |

Table 7
Intensity decay of S. Nuclease with increasing concentration of acrylamide

| [acrylamide] (M) | $\langle\tau\rangle$ ns | $\tau_i$ (ns) | $\alpha_i$ | $f_i$ | $\chi^2_R$ |
|---|---|---|---|---|---|
| 0 | 5.77 | 4.60 | 0.68 | 0.57 | |
| | | 7.31 | 0.32 | 0.43 | 1.2 |
| 0.05 | 4.94 | 2.79 | 0.29 | 0.18 | |
| | | 5.41 | 0.71 | 0.82 | |
| 0.20 | 3.57 | 1.26 | 0.14 | 0.05 | |
| | | 3.69 | 0.86 | 0.95 | 1.8 |
| 0.535 | 2.07 | 1.09 | 0.43 | 0.25 | |
| | | 2.40 | 0.57 | 0.75 | 2.4 |
| 0.833 | 1.57 | 0.42 | 0.44 | 0.16 | |
| | | 1.79 | 1.56 | 0.84 | 2.4 |
| 1.10 | 1.26 | 0.22 | 0.50 | 0.14 | |
| | | 1.42 | 0.50 | 0.86 | 2.7 |

Table 8
Global anisotropy during analysis of S. Nuclease, 20°C, with acrylamide quenching [a]

| Model | $\bar{\theta}$ (ns) | hw (ns) | $r_{0i}$ | $\chi^2_R$ |
|---|---|---|---|---|
| Lorentzian | 10.19 | 2.70 | 0.305 | 1.5 |
| | 9.91 | ⟨0.10⟩ [b] | 0.304 | 2.0 |
| Gaussian | 10.99 | 9.07 | 0.305 | 1.6 |
| | 9.89 | ⟨0.10⟩ | 0.303 | 2.0 |
| 1 exponential | 9.88 | – | 0.303 | 2.0 |
| 2 exponential | 0.09 | – | 0.018 | 1.0 |
| | 10.16 | | 0.301 | |

[a] Simultaneous analysis and data for six concentrations of acrylamide (Table 7). The differential phases and modulated anisotropy data are taken from ref. [53].
[b] The half-width was held constant at the value indicated in the angular brackets ⟨ ⟩.

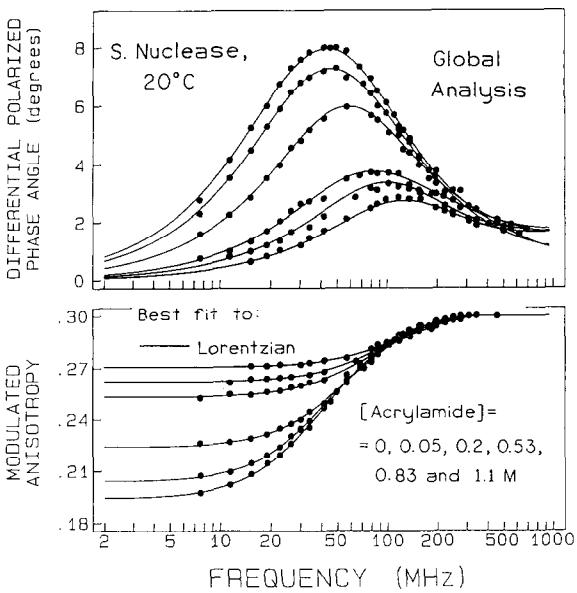


Fig. 5. Frequency-domain anisotropy data for S. Nuclease with increasing amounts of acrylamide quenching.

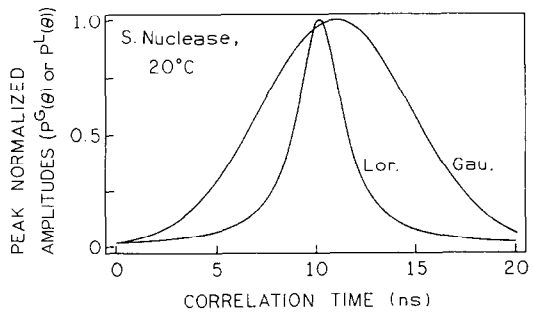


Fig. 6. Correlation time distributions from global analysis of the S. Nuclease data with acrylamide quenching.

beyond those of a Gaussian distributions [45]. In order to fit the data, the least squares algorithm most suppress these wings, which requires a more narrow half-width for the Lorentzian model.

### 4.4. Effects of temperature and GuHCl on the RNase $T_1$ anisotropy decay

The single tryptophan residue in RNase $T_1$ is thought to be rigidly contained within the protein structure [53,54]. In such cases one expects the anisotropy decay to display a single correlation time which is due to the hydrodynamic behavior of an equivalent rigid sphere, or a narrow multi-exponential distribution for an ellipsoid of revolution. We used RNase $T_1$ to determine the effects of gradual protein unfolding, which is expected to result in a more complex decay of anisotropy.

Temperature-dependent anisotropy data for RNase $T_1$ are shown in Fig. 7. At 5 and 20°C the rotational behavior appears to be well described by a single correlation time, without a significant distribution about the mean value. The FDA data of 5 and 20°C are equally well fit by the distribution models with narrow half-widths or by the single exponential model. Importantly, attempts to force fit the data to wider distributions (hw = 5 ns) result in elevated values of $\chi^2_R$ (Table 9). When the temperature is increased to 53°C, the

Table 9
Anisotropy decay analysis for the intrinsic tryptophan emission from RNase $T_1$, pH 5.5

| [GuHCl]/°C | Lorentzian | | | | Gaussian | | | | Multi-exponential | |
|---|---|---|---|---|---|---|---|---|---|---|
| | $\theta$ (ns) | hw (ns) | $r_0$ | $\chi^2_R$ | $\theta$ (ns) | hw (ns) | $r_0$ | $\chi^2_R$ | $\chi^2_R$(1 exp) | $\chi^2_R$(2 exp) |
| 0/5°C | 10.6 | 0.1 | 0.276 | 2.0 | 10.7 | 0.2 | 0.275 | 2.0 | 1.9 | 1.9 |
| | – | ⟨5⟩ | – | 4.7 | – | ⟨5⟩ | – | 2.3 | – | – |
| 1.5/5° | 9.2 | 2.3 | 0.275 | 1.7 | 9.8 | 7.5 | 0.274 | 1.6 | 2.5 | 1.8 |
| 3.0/5° | 4.8 | 5.4 | 0.275 | 1.1 | 5.6 | 10.4 | 0.276 | 1.3 | 19.7 | 1.0 |
| 3.0/5° | – | ⟨0.1⟩ | – | 19.0 | – | ⟨0.1⟩ | – | 19.7 | – | – |
| 0/20°C [a] | 6.6 | 1.5 | 0.312 | 1.5 | 7.0 | 5.1 | 0.312 | 1.4 | 1.8 | 1.5 |
| | – | ⟨0.1⟩ | – | 1.7 | – | ⟨0.1⟩ | – | 1.8 | – | – |
| 0/53°C | 0.9 | 1.9 | 0.249 | 2.9 | −5.4 | 9.3 | 0.257 | 2.1 | 356.5 | 0.8 |
| | – | ⟨0.1⟩ | – | 14.3 | – | ⟨0.1⟩ | – | 15.4 | – | – |

[a] Obtained from global analysis with acrylamide quenching (5 files, exc. 300 nm).

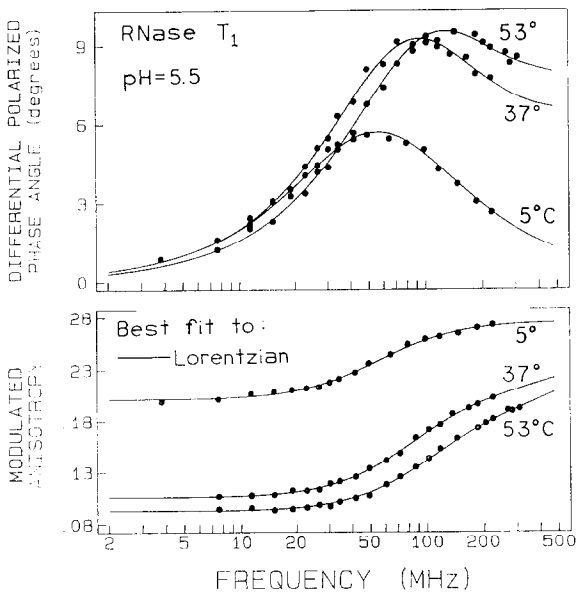


Fig. 7. Frequency-domain anisotropy data for RNase $T_1$ with increasing temperature.

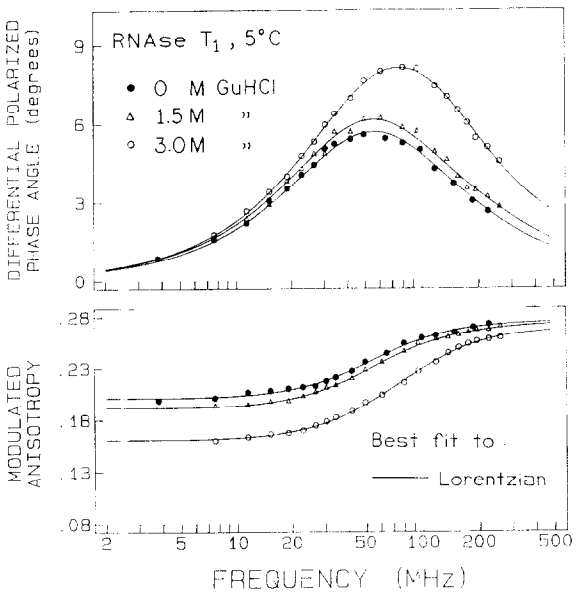


Fig. 9. Frequency-domain anisotropy data for RNase $T_1$ with increasing concentrations of GuHCl.

anisotropy decay appears to display a wide range of correlation times (Fig. 8).

Unfolding of RNase $T_1$ by GuHCl (Fig. 9) also results in a distribution of correlation times. This is seen from the distributions resulting from the analyses (Fig. 10), and from the force fits to narrow distributions which result in elevated values of $\chi^2_R$ (Table 9). We questioned whether the

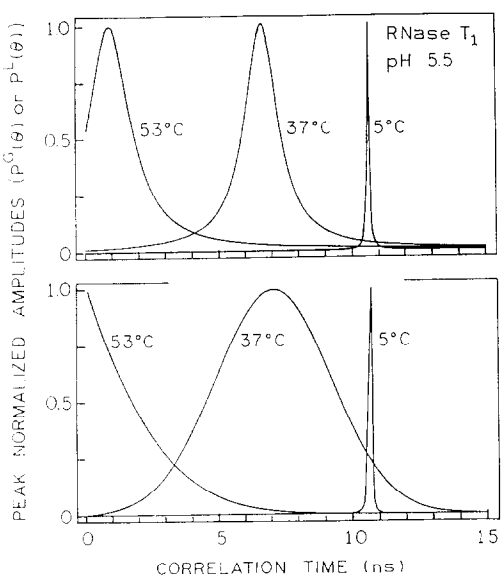


Fig. 8. Correlation-time distributions for RNase $T_1$ with increasing temperature. The data used to recover $P(\theta)$ at 5 and 53°C were published elsewhere [52]. The top panel shows the Lorentzian fit, and the bottom panel shows the Gaussian fit.

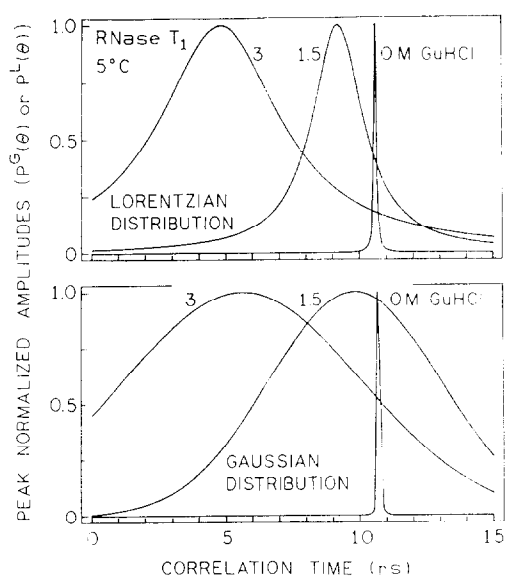


Fig. 10. Correlation-time distributions for RNase $T_1$ with increasing concentration of GuHCl.

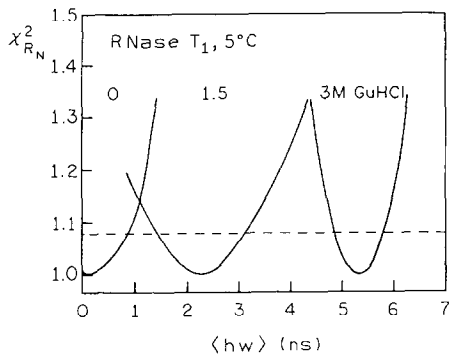


Fig. 11. $\chi^2_R$ surfaces of half width of Lorentzian distribution for RNase $T_1$ with increasing concentration of GuHCl. The other parameters ($\bar{\theta}$ and $r_0$) were floating during the analysis.

increases in distribution half-widths induced by GuHCl were reliably determined from the data. Hence, we examined the $\chi^2_R$ surfaces for the half-widths (Fig. 11). In determining these surfaces the half-width was held constant at the value indicated in the $x$ axis, and the value of $r_0$ and $\bar{\theta}$ were allowed to vary to minimize $\chi^2_R$. These surfaces show that the half-widths are in fact well determined from these data. For instance, for the native protein at 5°C (0 M GuHCl) a correlation time half-width larger than 1 ns is not consistent with the data. Conversely, with 3 M GuHCl, a half-width below 4.5 ns is not consistent with the data.

## 5. Conclusions

The anisotropy decays of peptides and proteins appear to be described by a distribution of correlation times, and correlation time distribution can be used to visualize the dynamics of proteins. In the case of single tryptophan proteins the widths of the distributions are sensitive to the structure of the proteins, and appear to increase as the proteins are unfolded by increased temperature or denaturants. Additional experimental and theoretical studies are required to interpret these distributions in terms of the molecular dynamics of proteins.

## Acknowledgement

Supported by Grants DMB-8804931 from the National Science Foundation and GM-39617 from the National Institutes of Health. Supported in part by the Medical Biotechnology Center at the University of Maryland. The authors thank Professor Maurice Eftink for providing the sample of RNase $T_1$, Professor Ludwig Brand for providing S. Nuclease, and Dr. Józef Kuśba for discussions on the theory and analysis.

## References

[1] G.G. Belford, R.L. Belford and G. Weber, Proc. Natl. Acad. Sci. 69 (1972) 1392–1393.
[2] T.J. Chuang and K.B. Eisenthal, J. Chem. Phys. 57 (1972) 5094–5097.
[3] M. Ehrenberg and R. Rigler, Chem. Phys. Letters 14 (1972) 539–544.
[4] E.W. Small and I. Eisenberg, Biopolymers 16 (1977) 1907–1928.
[5] R.F. Steiner, in: Topics in fluorescence spectroscopy, Vol. 2. Principles, ed. J.R. Lakowicz (Plenum Press, New York, 1991) pp. 1–52.
[6] J.R. Lakowicz, Principles of fluorescence spectroscopy (Plenum Press, New York, 1983) pp. 115–185.
[7] M.D. Barkley and B.H. Zimm, J. Chem. Phys. 70 (1979) 2991–3007.
[8] Allison, S.A. and J.M. Schurr, Chem. Phys. 41 (1979) 35–59.
[9] J.C. Thomas, S.A. Allison, C.S. Appellof and J.M. Schurr, Biophys. Chem. 12 (1980) 177–188.
[10] D.P. Millar, R.J. Robbins and A.H. Zewail, J. Chem. Phys. 76 (1982) 2080–2094.
[11] D.P. Millar, R.J. Robbins and A.H. Zewail, Proc. Natl. Acad. Sci. 77 (1980) 5593–5597.
[12] D. Magde, M. Zappala, W.H. Knox and T.M. Nordlund, J. Phys. Chem. 87 (1983) 3286–3288.
[13] I. Ashikawa, K. Kinosita, A. Ikegami, Y. Nishimura, M. Tsuboi, K. Watanabe, K. Iso and T. Nakano, Biochemistry 22 (1983) 6018–6026.
[14] I. Ashikawa, T. Furuno, K. Kinosita, A. Ikegami, H. Takahashi and H. Akutsu, J. Biol. Chem. 259 (1984) 8338–8344.
[15] I. Ashikawa, K. Kinosita and A. Ikegami, Biophys. Acta 782 (1984) 87–93.
[16] K. Kinosita, S. Kawato and A. Ikegami, Biophys. J. 20 (1977) 289–305.
[17] G. Lapari and A. Szabo, Biophys. J. 30 (1980) 489–506.
[18] W. van der Meer, H. Pottel, W. Herrmann, M. Ameloot, H. Hendricks and M. Schröder, Biophys. J. 5 (1984) 515–523.

[19] M. Ameloot, H. Hendricks, W. Herrmann, H. Pottel, F.V. Cauwelaert and W. van der Meer, Biophys. J. 45 (1984) 525–539.
[20] M.R. Eftink, Topics in fluorescence spectroscopy, Vol. 2. Principles, ed. J.R. Lakowicz (Plenum Press, New York, 1991) pp. 53–126.
[21] I. Munro, I. Pecht and L. Stryer, Proc. Natl. Acad. Sci. 65 (1979) 823–830.
[22] J. Yguerabide, H.F. Epstein and L. Stryer, J. Mol. Biol. 51 (1970) 573–590.
[23] R.D. Ludescher, I.D. Johnson, J.J. Volwerk, G.H. de Haas, P.C. Jost and B.S. Hudson, Biochemistry 27 (1988) 6618–6628.
[24] D.R. James, D.R. Demmer, R.P. Steer and R.E. Verra, Biochemistry 24 (1985) 5517–5526.
[25] T.M. Nordlund and D.M. Podolski, Photochem. Photobiol. 38 (1983) 665–669.
[26] J.R. Lakowicz, I. Gryczynski and H. Cherek, J. Biol. Chem. 261 (1984) 2240–2245.
[27] B.P. Maliwal and J.R. Lakowicz, Biochim. Biophys. Acta 873 (1986) 173–181.
[28] J.R. Lakowicz, G. Laczko and I. Gryczynski, Biochemistry 26 (1987) 82–90.
[29] M. Karplus, Internal dynamics of proteins, Methods in Enzymology Vol. 131 (Academic Press, New York, 1986) pp. 283–307.
[30] M. Karplus and J.A. McCammon, CRC Crit. Rev. Biochem. 9 (1981) 293–349.
[31] L.S. Liebovitch, J. Fishbarg, J.P. Koniarek, I. Todorova and M. Wang, Biochim. Biophys. Acta 896 (1987) 173–180.
[32] R. Kopelman, J. Phys. (Paris) 46 (1985) C7–9.
[33] D.R. James and W.R. Ware, Chem. Phys. Letters 120 (1985) 455–459.
[34] D.R. James, Y.S. Liu, P. DeMayo and W.R. Ware, Chem. Phys. Letters 120 (1985) 460–465.
[35] D.R. James and W.R. Ware, Chem. Phys. Letters 126 (1986) 7–11.
[36] J.R. Alcala, E. Gratton and F.G. Prendergast, Biophys. J. 51 (1987) 587–596.
[37] J.R. Alcala, E. Gratton and F.G. Prendergast, Biophys. J. 51 (1987) 597–604.
[38] J.R. Alcala, E. Gratton and F.G. Prendergast, Biophys. J. 51 (1987) 925–936.
[39] J.R. Lakowicz, H. Cherek, I. Gryczynski, N. Joshi and M.L. Johnson, Biophys. Chem. 28 (1987) 35–50.
[40] I. Gryczynski, H. Cherek and J.R. Lakowicz, Biophys. Chem. 30 (1988) 271–277.
[41] J.R. Lakowicz, H. Cherek, I. Gryczynski, N. Joshi and M.L. Johnson, Biophys. J. 51 (1987) 755–768.
[42] J.R. Lakowicz, I. Gryczynski and W. Wiczk, Chem. Phys. Letters 49 (1988) 134–139.
[43] J.M. Beechem, M. Ameloot and L. Brand, Chem. Phys. Letters 120 (1985) 466–472.
[44] J.M. Beechem, E. Gratton, M. Ameloot, J.R. Knutson and L. Brand (1991) Topics in Fluorescence Spectroscopy. Vol. 2. Principles, ed. J.R. Lakowicz (Plenum Press, New York, 1991) pp. 241–305.
[45] P.R. Bevington, Data reduction and error analysis for the physical sciences (McGraw-Hill, New York, 1969).
[46] J.R. Lakowicz, E. Gratton, G. Laczko, H. Cherek and M. Limkeman, Biophys. J. 46 (1984) 463–467.
[47] I. Gryczynski, H. Cherek, G. Laczko and J.R. Lakowicz, Chem. Phys. Letters 135 (1987) 193–199.
[48] J.R. Lakowicz, H. Cherek, J. Kuśba, I. Gryczynski and M.L. Johnson, J. Fluorescence 3 (1993) 103–115.
[49] G. Weber, J. Chem. Phys. 66 (1977) 4081–4091.
[50] J.R. Lakowicz, G. Laczko and I. Gryczynski, Rev. Sci. Instr. 57 (1986) 2499–2506.
[51] G. Laczko, J.R. Lakowicz, I. Gryczynski, Z. Gryczynski and H. Malak, Rev. Sci. Instr. 61 (1990) 2331–2337.
[52] I. Gryczynski, M. Eftink and J.R. Lakowicz, Biochim. Biophys. Acta 954 (1988) 244–252.
[53] J.R. Lakowicz, I. Gryczynski, H. Szmacinski, H. Cherek and N. Joshi, Eur. Biophys. J. 19 (1991) 125–140.
[54] D.R. James, D.R. Dremmer, R.P. Steer and R.E. Verral, Biochem. 24 (1985) 5517–5526.